Supplementary Materials

High-Performance Long-wave Infrared Photodetector Based on $WSe_2/PdSe_2$ Broken-Gap Heterodiode

Suofu Wang[1+], Yajie Bai[1+], Mingli Liu[1+], Xiaolan Zong[2], Wenhui Wang[2], Qingge Mu[1], Tao Han[1], Feng Li[1], Shaoliang Wang[1], Lei Shan[1*], and Mingsheng Long[1*]

1. Information Materials and Intelligent Sensing Laboratory of Anhui Province, Key Laboratory of Structure and Functional Regulation of Hybrid Materials of Ministry of Education, Institutes of Physical Science and Information Technology, Anhui University, 111 Jiu Long Road, Hefei 230601, China
2. Institute for Quantum Control and Quantum Information, School of Physics and Materials Engineering, Hefei Normal University, Hefei 230601, China
3. School of Physics, Southeast University, Nanjing 211189, China

Corresponding authors: M. L. (longms@ahu.edu.cn), L. S. (lshan@ahu.edu.cn)

Keywords: Photodetector, Tungsten diselenide, Palladium diselenide, Heterodiode, Long-wave infrared

1. $PdSe_2$ single crystal growth and characterization

The self-flux method was used to synthesize $PdSe_2$ single crystals. Pd (99.99%), and Se (99.99%) powders were weighed by an atomic ratio of Pd: Se = 1: 6. And the excessive selenium is to prevent selenium defects resulting in synthetic impure samples. The fully mixed powder was sealed in a vacuum quartz ampoule. The sample was placed in a box furnace. The temperature was rising to 800 °C for 2 hours, and then hold at 800 °C for 5 hours. To make Pd react fully, the furnace was further increased to 1050 °C and held at 1050 °C for 2 hours. Whereafter, the temperature was cooled down to 850 °C within two hours. Finally, to ensure the smooth growth of samples, the furnace temperature was slowly reduced to 450 °C at a speed of 5.5 °C/h. And then the furnace power supply was turned off, and naturally cooled to room temperature. A single crystal with a metallic luster and several millimeters in size was obtained. Raman spectra of $PdSe_2$ and WSe_2 were carried out using a 532 nm laser as excitation light. For $PdSe_2$, four distinct peaks are located in ~143.5 cm^{-1}, ~205 cm^{-1}, ~221 cm^{-1}, and ~257.4 cm^{-1} corresponding to the A_g^1-B_{1g}^1, A_g^2, B_{1g}^2, and A_g^3 modes, respectively.[1-3] There are some second-order and combinational modes in the Raman spectrum of WSe_2 bulk crystal. Two strong peaks around 250 cm^{-1} are assigned to E_{2g}^1 and A_{1g} modes, respectively.[4]

2. Device fabrication and measurements

The thin flakes of WSe_2 and $PdSe_2$ were obtained from bulk single crystals by mechanically exfoliating. The thicknesses of the samples were identified by an optical microscope. Then the samples were transferred to pre-patterned electrodes on silicon substrates using the dry transfer technique. The silicon substrates were covered by a 280 nm layer of thermal oxide. The electrodes were fabricated through the standard electron beam lithography (EBL) and followed by electron beam evaporation 5 nm Ti/25 nm Au. A dual-channel digital source meter (Keithley 2636B) was used as a voltage source. Single wavelength lasers of 405 nm, 520 nm, and 637 nm were used to evaluate the performance of the $WSe_2/PdSe_2$ in the visible range. The lasers were focused on the device using a 20× objective lens. A wavelength-tuneable homemade mid-wave infrared (MWIR) laser (ranging from 2.5 μm to 4.2 μm) and a long wavelength infrared (LWIR) laser of 10.6 μm were used to study the uncooled MWIR and LWIR photoresponse of the $WSe_2/PdSe_2$ heterodiode. The noise current density spectrum at different biases was acquired in a metal-shielded box by using a noise measurement system (PDA NC300L, 100 kHz bandwidth).

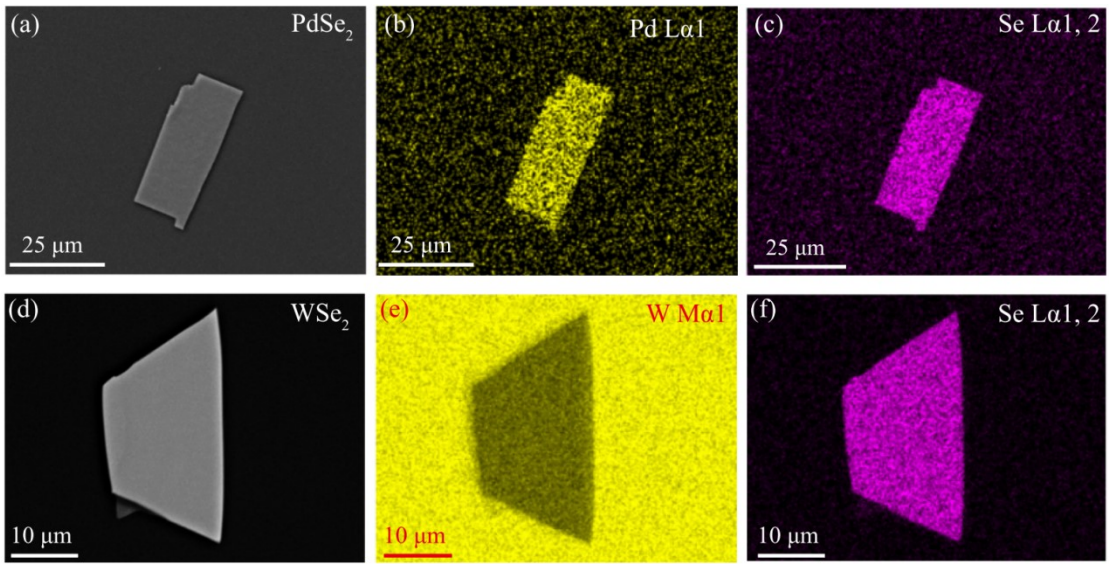

Figure S1. SEM image and EDS elements mappings. (a) and (d) SEM images of $PdSe_2$ and WSe_2 flakes. (b) and (c) Uniform distribution of Pd and Se elements in the EDS mappings. (e) and (f) EDS element mappings with uniform distribution of W and Se.

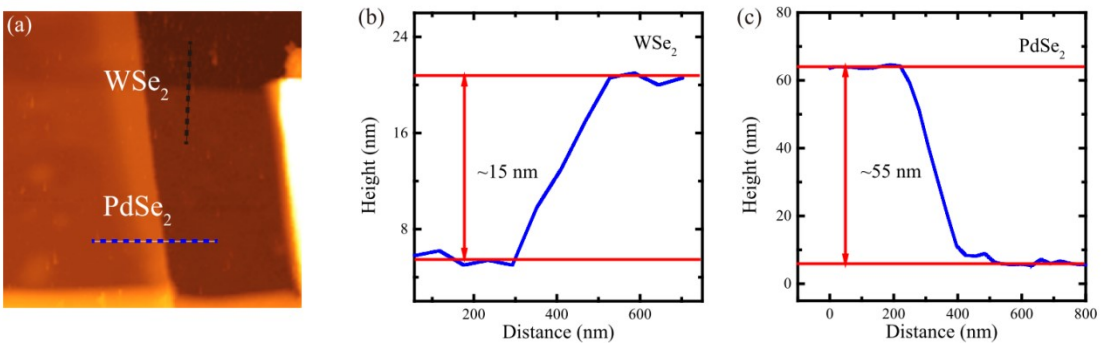

Figure S2. AFM image and the thickness of the WSe_2 and $PdSe_2$ flakes. (a) AFM image of a measured $WSe_2/PdSe_2$ heterodiode device. (b) and (c) The thicknesses of the WSe_2 and $PdSe_2$ flakes of a $WSe_2/PdSe_2$ heterodiode device.

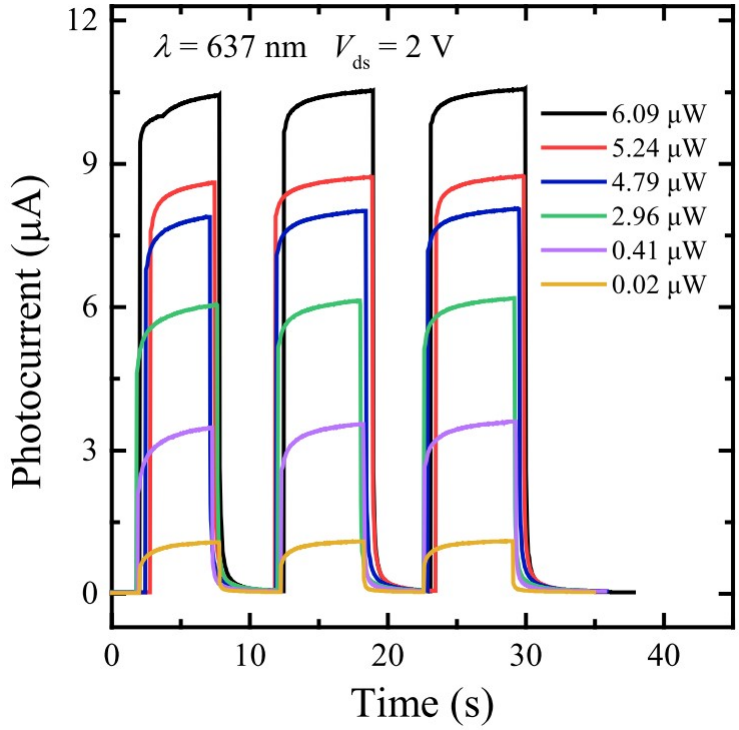

Figure S3. Temporal photoresponse of the $WSe_2/PdSe_2$ heterodiode device under 637 nm laser at a bias of 2 V.

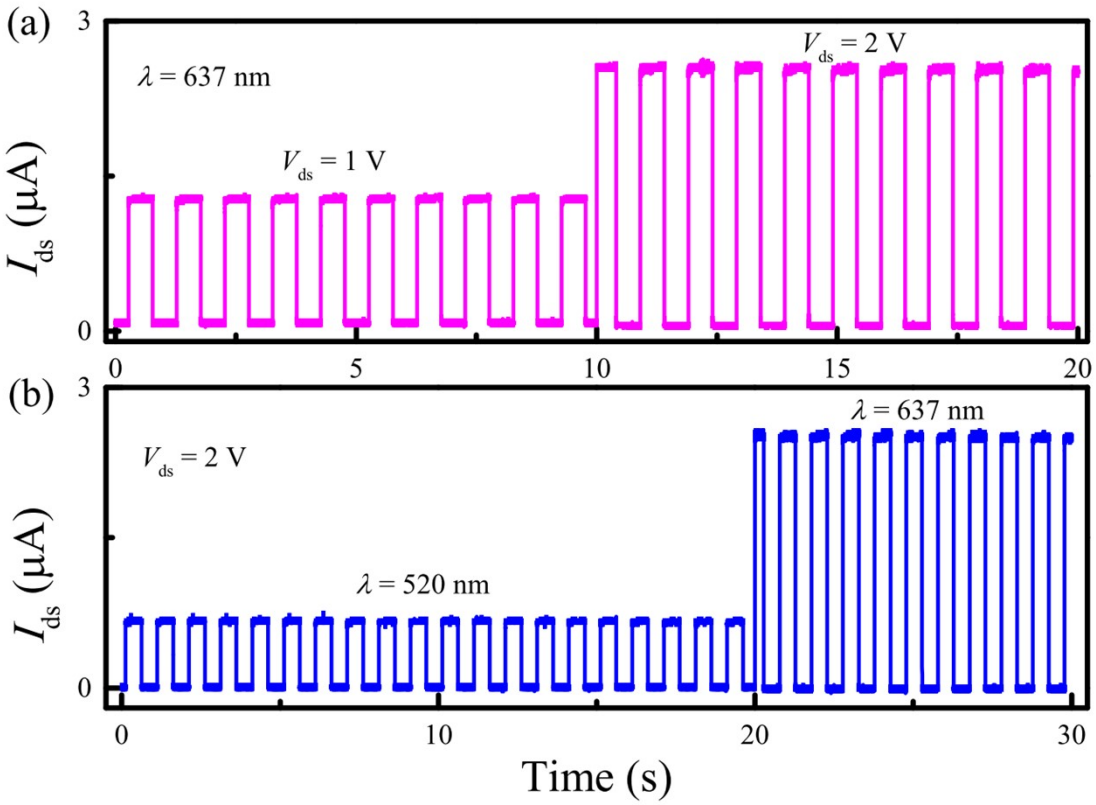

Figure S4. The temporal photoresponse of the $WSe_2/PdSe_2$ heterodiode device. (a) Bias voltage dependence of photoresponse at 637 nm laser. (b) Temporal photoresponse of the $WSe_2/PdSe_2$ heterodiode device under 520 nm and 637 nm lasers at a bias of 2 V.

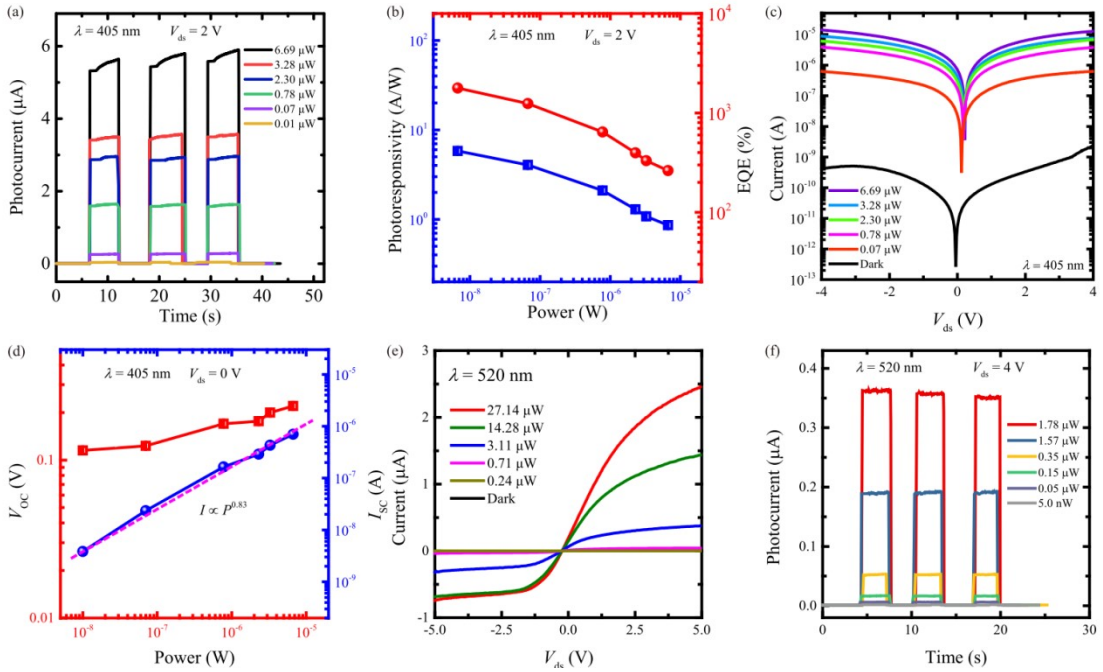

Figure S5. Photoresponse of the $WSe_2/PdSe_2$ heterodiode device in the visible spectral range. (a) Temporal photoresponse of the device with various powers of 405 nm laser at a bias of 2 V. (b) The extracted *R* and EQE of the device as a function of illumination power of 405 nm laser at 2V bias. (c) Output characteristic curves of the $WSe_2/PdSe_2$ heterodiode device under a 405 nm laser with varying light power. (d) Extracted V_{OC} and I_{SC} as a function of incident illumination power of 405 nm laser. (e) The *I-V* curves of the typical device with various light power of 520 nm laser. (f) The temporal photoresponse under various incidence light powers of the 520 nm laser at a bias of 4 V.

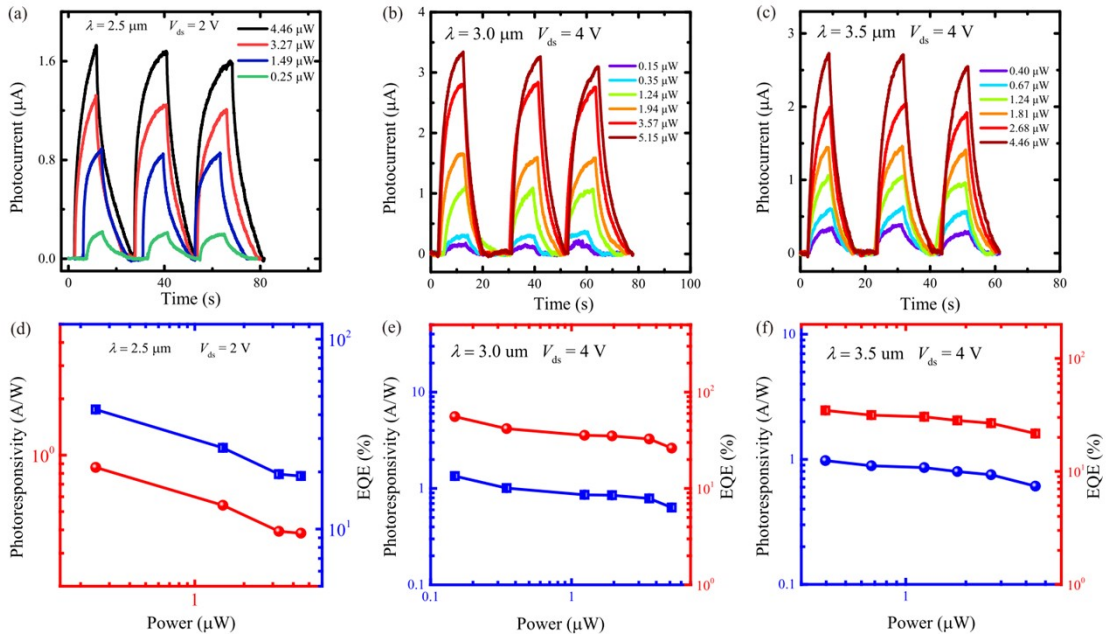

Figure S6. Photoresponse of the $WSe_2/PdSe_2$ heterodiode device at MWIR spectral range. (a)-(c) Temporal photoresponse of the device with different illumination powers of 2.5 μm, 3.0 μm, and 3.5-μm laser. (d)-(f) Extracted *R* (left axis) and EQE (right axis) versus incident light power of 2.5 μm, 3.0 μm, and 3.5 μm laser, respectively.

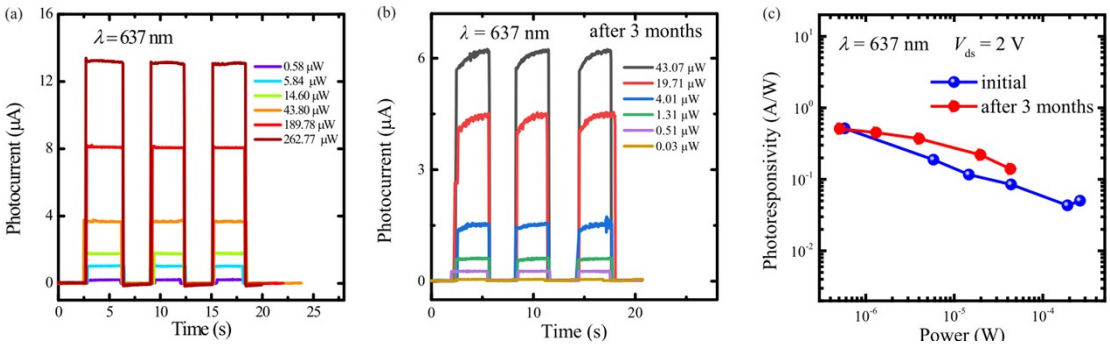

Figure S7. The stability of the $WSe_2/PdSe_2$ heterodiode device. (a) and (b) Temporal photoresponse of the $WSe_2/PdSe_2$ heterodiode device under various incident light power of the 637-nm laser at 2 V bias of a newly fabricated device and exposed in the air for more than 3 months, respectively. (c) *R* versus incident light power of the twice measured results.

Table. S1. Summarized the performance of 2D materials photodetectors

Materials	λ [μm]	R [A/W]	Bias (V)	Time τ_r/τ_d (μs)	D^*[Jones]	On/off ratio	rectification ratio	Ref.
$PdSe_2$	0.532	0.0036	1	11/6 ms	--	10^2	--	5
$PdSe_2$	0.45-10.6	249.1-42.6	1	51.3/53.7	7×10^8 1.1×10^9	10^3	--	6
WSe_2	0.65	0.36	1	310/930 (ms)	1×10^9	＜10	--	7
WSe_2/MoS_2	0.532	0.011	-1	--	--	75	50	8
$PdSe_2/MoS_2$	0.637（0.45-10.6）	11.15	1	--	＜10^{10}	＜10	10^2	6
Bp/MoS_2	0.532（1.55）	22.3-0.153	-2	15	3.1×10^{11} 2.13×10^9	10^2	10^3	9
$MoS_2/CdTe$	0.78（0.2-1.7	0.036	--	43.7/82.1	6.1×10^{10}	3×10^4	＜10^2	10
$PdSe_2/Bp$	0.637（0.4-10.6）	60.3	1	2.9/4.0	2.05×10^9	＜10	＜10	11
WSe_2/WSe_2	0.532	0.0112	0	--	--	--	--	12
$PdSe_2/MoSe_2$	0.532	0.651	--	41.7/62.5	5.29×10^{11}	--	5.6×10^3	13
PtS_2/WSe_2	0.532-0.92	1.7	1	8	3.8×10^{10}	10^5	10^8	14
BP/MoS_2	633	0.418	-2	--	--	--		15
WSe_2/G	520	6.62×10^{-2}	--	--	--	--	--	16
$MoTe_2/MoS_2$	473	0.064	2	--	--	--	--	17
BP/WSe_2	1.55（0.637-1.55）	0.5	0.5	800	10^{10}	10^3	＞10^3	18
b-As-MoS_2	0.4-8.05	0.22	--	540/520	--	--	--	19
Te/ReS_2	0.632	180	--	5 ms	10^9	--	--	20

Te/ReS_2	0.66	2.45	-1	11.9/42.5	4.74×10^{9}	8.32×10^{1}	10^{3}	21
Te/WS_2	0.635	3.69	-2	9.5/9.1	1.34×10^{12}	1.48×10^{3}	--	22
Te/InSe	0.4	0.45	-2	0.6/0.8	1.1×10^{13}	10^{4}	--	23
$PtSe_2$/Ge	1.550	0.602	0	7.42/16.71	6.31×10^{11}	3.8×10^{3}	~25	24
Graphene/Ge	1.55	0.0518	0	23/108	1.38×10^{10}	1×10^{4}	~24	25
WSe_2/$PdSe_2$	**0.4-10.6**	**55.3-0.29**	**2**	**70/60**	**3.5×10^{10} 5.9×10^{8}**	**$\sim10^{6}$**	**10^{3}**	**This work**

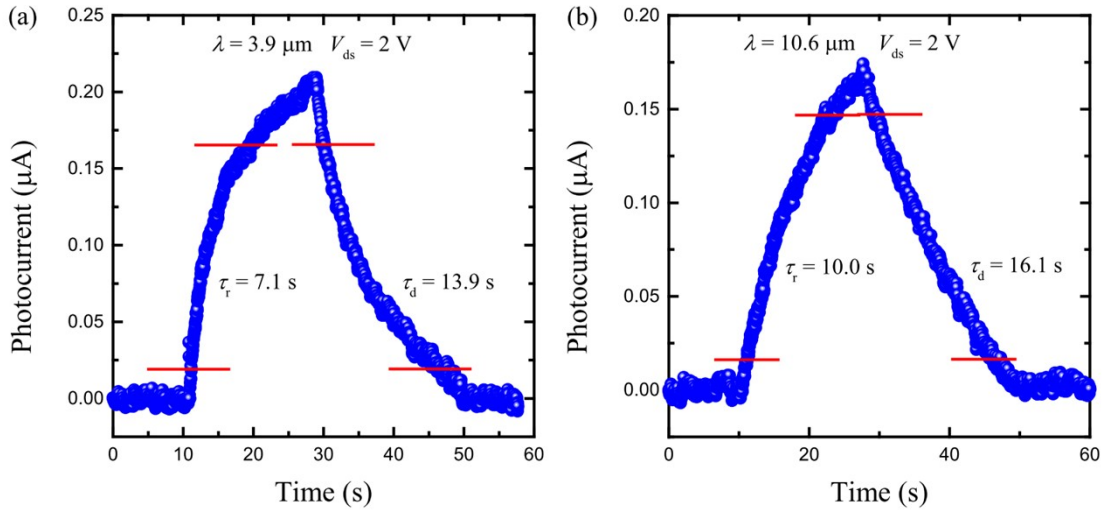

Figure S8 Photoresponse time of the $WSe_2/PdSe_2$ heterodiode device. (a) and (b) the speed of the $WSe_2/PdSe_2$ heterodiode device under MWIR 3.9 μm and LWIR 10.6 μm at 2 V bias, respectively.

References

1 L. H. Zeng, D. Wu, S. H. Lin, C. Xie, H. Y. Yuan, W. Lu, S. P. Lau, Y. Chai, L. B. Luo, Z. J. Li, and Y. H. Tsang, Adv. Funct. Mater., 2019, 29, 1806878.

2 W. L. Chow, P.Yu, F. C. Liu, J. H. Hong, X. L. Wang, Q. S. Zeng, C. H. Hsu, C. Zhu, J. D. Zhou, X. W.Wang, J. Xia, J. X. Yan, Y. Chen, D. Wu, T. Yu, Z. X. Shen, H. Lin, C. H. Jin, B. K. Tay, and Z. Liu, Adv. Mater., 2017, 29, 1602969.

3 A. D. Oyedele, S. Z. Yang, L. B. Liang, A. A. Puretzky, K. Wang, J. J. Zhang, P. Yu, P. R. Pudasaini, A. W. Ghosh, Z. Liu, C. M. Rouleau, B. G. Sumpter, M. F. Chisholm, W. Zhou, P. D. Rack, D. B. Geohegan, and K. Xiao, J. Am. Chem. Soc., 2017, 139, 14090-14097.

4 H. Li, G. Lu, Y. Wang, Z. Y. Yin, C. Cong, Q. He, L. Wang, F. Ding, T. Yu, H. Zhang, Small 2013, 9, 1974-1981.

5 J. Zhong, J. Yu, L. Cao, C. Zeng, J. Ding, C. Cong, Z. Liu, Y. Liu, Nano Res., 2020, 13, 1780-1786.

6 M. Long, Y. Wang, P. Wang, X. Zhou, H. Xia, C. Luo, S. Huang, G. Zhang, H. Yan, Z. Fan, et al, ACS Nano., 2019, 13, 2511-2519.

7 H. Chao, et al, Adv. Funct. Mater., 2017, 27, 1603605.

8 F, Marco M., et al. Nano Lett., 2014, 14, 4785-4791.

9 L. Ye, H. Li, Z. F. Chen, J. B. Xu, ACS Photonics., 2016, 3, 692-699.

10 Y. G.Wang, X. W. Huang, D. Wu, R. R. Zhuo, E. P. Wu, C. Jia, Z. F. Shi, T. T. Xu, Y. T. Tian, X. J. Li, J. Mater. Chem. C., 2018, 6, 4861-4865.

11 Q. Dong, F. Wang, X. Hu, Y. Lu, D. Zhao, M. Zhang, T. Han, X. Hou, S.Wang, M. Long and L. Shan, Appl. Phys. Lett. 2022, 120, 231103.

12 C. Tan, H. Wang, X. Zhu, W. Gao, H. Li, J. Chen, G. Li, L. Chen, J. Xu, X. Hu, et al, ACS Appl. Mater. Interfaces., 2020, 12, 44934-44942.

13 J. Zhong, B. Wu, Y. Madoune, Y. Wang, Z. Liu, Y. Liu, Nano Res., 2022, 15, 2489-2496.

14 C. Tan, S. Yin, J. Chen, Y. Lu, W. Wei, H. Du, K. Liu, F. Wang, T. Zhai, and L. Li, ACS Nano., 2021, 15, 8328.

15 Y. Deng, Z. Luo, N. J. Conrad, H. Liu, Y. Gong, S. Najmaei, P. M. Ajayan, J. Lou,

X. Xu, P. D. Ye, ACS Nano., 2014, 8, 8292-8299.

16 A. Gao, E. Liu, M. Long, W. Zhou, Y. Wang, T. Xia, W. Hu, B. Wang, F. Miao, A ppl. Phys. Lett., 2016, 108, 223501.

17 F. Wang, L.Yin, Z. X. Wang, K. Xu, F. M. Wang, T. A. Shifa, Y. Huang, C. Jiang, J.He, Adv. Funct. Mater., 2016, 26, 5499-5506.

18 L.Ye, P. Wang, W. Luo, F. Gong, L. Liao, T. Liu, L. Tong, J. Zang, J. Xu, W.Hu, Nano Energy., 2017, 37, 53-60.

19 M. Long, A. Gao, P. Wang, H. Xia, C. Ott, C. Pan, Y. Fu, E. Liu, X. Chen, W. Lu, et al, Sci. Adv. 2017, 3, e1700589.

20 J. Tao, J. Jiang, S. Zhao, Y. Zhang, X. Li, X. Fang, P. Wang, W. Hu, Y. H. Lee, H. Lu, et al, ACS Nano., 2021, 15, 3241-3250.

21 Y. F. Yan, M. X. Li, K. X, K. M. Yang, D. Wu, L. Li, G. T. Fei, W. Gan, Nanosca le., 2023, 15, 7730–7736.

22 L. Han, M. Yang, P. Wen, W. Gao, N. Huo and J. Li, Nanoscale Adv., 2021, 3, 265 7-2665.

23 F. Qin, F. Gao, M. Dai, Y. Hu, M. Yu, L. Wang, W. Feng, B. Li and P. Hu, ACS Appl. Mater. Interfaces., 2020, 12, 37313-37319.

24 L. Wang, et al, J. Mater. Chem. C., 2019, 7, 5019-5027.

25 L. H. Zeng, M. Z. Wang, H. Hu, B. Nie, Y. Q. Yu, C. Y. Wu, L. Wang, J. G. Hu, C. Xie, F. X. Liang and L. B. Luo, ACS Appl. Mater. Interfaces., 2013, 5, 9362-9366.